

Study of size effect in silicon nanostructures using Raman spectroscopy

A THESIS

*Submitted in partial fulfillment of the
requirements for the award of the degree
of*
Master of Science

by
Manushree Tanwar



DISCIPLINE OF PHYSICS
INDIAN INSTITUTE OF TECHNOLOGY INDORE
JUNE 2018



INDIAN INSTITUTE OF TECHNOLOGY INDORE

CANDIDATE'S DECLARATION

I hereby certify that the work which is being presented in the thesis entitled “**STUDY OF SIZE EFFECT IN SILICON NANOSTRUCTURES USING RAMAN SPECTROSCOPY**” in the partial fulfillment of the requirements for the award of the degree of **MASTER OF SCIENCE** and submitted in the **DISCIPLINE OF PHYSICS, Indian Institute of Technology Indore**, is an authentic record of my own work carried out during the time period from July 2016 to June 2017 under the supervision of **Dr. Rajesh Kumar**, Associate Professor, Indian Institute of Technology Indore

The matter presented in this thesis has not been submitted by me for the award of any other degree of this or any other institute.

**Signature of the student with date
(Manushree Tanwar)**

This is to certify that the above statement made by the candidate is correct to the best of my/our knowledge.

Signature of the Supervisor
Dr. Rajesh Kumar

Manushree Tanwar has successfully given her M.Sc. Oral Examination held on **19th June 2018**

Signature of Supervisor of MSc thesis
Date:

Convener, DPGC
Date:

Signature of PSPC Member
Date:

Signature of PSPC Member
Date:

ACKNOWLEDGEMENTS

Firstly, I would like to express my sincere gratitude to my advisor **Dr. Rajesh Kumar** for the continuous support in my M.Sc. project study and related research, for his patience, motivation, and immense knowledge. His guidance helped me in all the time of research and writing of this thesis. I could not have imagined having a better advisor and mentor for my M.Sc. project.

I would like to thank my PSPC member Dr. Preeti A. Bhoje and Dr. Vinod Kumar.

I am highly thankful to all the members of the magnetic and semiconducting lab for the stimulating discussions, supporting me and guiding me throughout whenever I needed them.

I am highly thankful to Sophisticated Instrumentation Centre (SIC) at IIT Indore for SEM measurements as without their support this report would not be possible.

Finally, I must express my very profound gratitude to my parents for providing me with unfailing support and continuous encouragement throughout my years of study and through the process of researching and writing this thesis. This accomplishment would not have been possible without them.

Manushree Tanwar

***Dedicated to my
parents and teacher***

Abstract

The present thesis focuses on fabrication of Silicon nanostructures using Metal Induced Etching and its characterization using Raman spectroscopy. Various theoretical models have been analyzed which explain the perturbation induced due to the confinement. Experimental results were then confirmed using Scanning Electron Microscopy (SEM) and the theoretical models for the Raman line-shape of silicon nanostructures, to find out the surface morphology and the effect of quantum confinement. Comparison of two models PCM (Phonon confinement model) and MPCM (Modified Phonon Confinement Model) have been done in order to choose the suitable confinement function to account for this perturbation. Though the MPCM is not able to explain the confinement in an appropriate manner but an anomaly of broadened line shape when the size is reduced below 1 nm is observed. Furthermore, theoretical model for the Raman line shape for amorphous silicon has been proposed in order to extract the information lying under the envelope of amorphous line-shape. Also, due to the similarity between the relaxation of $k \sim 0$ selection rule in case of both amorphous and silicon nanostructures, a relation of size dependence on Raman shift has been proposed in line with Silicon column and Silicon sphere, which existed earlier. Considering that the amorphous silicon has no predominant crystalline structure and is a messy lattice, the size obtained from both the two models have been prescribed as the short range order in amorphous silicon in which the atoms vibrate with random frequency thus generating random phonons and showing a broadened Raman line-shape due to the overlap of spectra from each atom. Therefore a two-fold approach has been adopted to validate the short range order obtained and a close agreement between the values is observed.

LIST OF PUBLICATIONS

1. M. Tanwar, P. Yogi, S. Lambora, S. Mishra, S. K. Saxena, P. R. Sagdeo, A. S. Krylov & R. Kumar, Generalisation of phonon confinement model for interpretation of Raman line-shape from nanosilicon, *Advances in materials and Processing Technologies*, (2017), **DOI**:10.1080/2374068X.2017.1413527.

TABLE OF CONTENTS

LIST OF FIGURES	viii-ix
LIST OF TABLES	x
ACRONYMS	xi
Chapter 1: Introduction	1-3
Chapter 2: Theoretical & Historical Background	4-8
2.1 Silicon (Si) and its structure	
2.2 Band diagram of silicon	
2.2.1 Effect of quantum confinement	
Chapter 3: Methods & Experimental Details	9-17
3.1 Field emission scanning electron microscope (FESEM)	
3.1.1 Types of signals generated	
3.1.2 Instrumentation part	
3.2 Raman Spectrometer	
3.3 Sample preparation	
3.3.1 Method used for preparation	
3.4 Metal Induced Etching Mechanism	
Chapter 4: Results and Discussions	18-37
4.1 Phonon Confinement Models	
4.2 Study of Raman Spectra from Crystalline, microcrystalline and amorphous Silicon	
4.2.1 Raman spectra from c-silicon	
4.2.2 Raman spectra from SiNWs	
4.2.3 Raman spectra from a-Si	

4.2.4 Estimation of short range order in a-Si using Raman scattering

Chapter 5: New findings, conclusions and future scope **38-39**

References **40**

LIST OF FIGURES

2.1	Silicon crystal structure	5
2.2	The values and notations of certain important k -points	5
2.3	A typical band structure of Si	6
3.1	Schematic of FESEM	9
3.2	Schematic of Raman Spectrometer	13
3.3	Block diagram of MIE mechanism. (a) Ag nanoparticle coated Si wafer. (b), (c) and (d) etching in HF + H ₂ O ₂ solution	15
3.4(a)	Cleaned silicon wafer	15
3.4(b)	Ag NPs deposited on silicon wafer.	15
3.5 (a)	Surface morphology of etched Si surface and cross-sectional view (insight) of AgN001	16
3.5(b)	Surface morphology of etched Si surface and cross-sectional view (insight) of AgP001	16
4.1	Raman shifts vs. size for Si spheres and columns	20
4.2	Raman shifts vs size obtained from MPCM	22
4.3	Raman spectra simulated from PCM equation	24
4.4	Asymmetry ratio vs size for MPCM and PCM	25
4.5	Fitting of experimentally observed Raman scattering data (discrete points by using equation(4.8) and (4.9)	26
4.6	Raman spectra for c-silicon(bulk)	28
4.7	Raman spectra for different SiNWs size obtained from equation	29
4.8	Illustration for depicting various Raman processes involving the scattering from c-Si, n -Si and a -Si.	31

4.9	Raman spectra of a-Si of samples AS1	33
4.10	Raman spectra of a-Si of samples AS2	34
4.11	Theoretically obtained Raman line shapes for (a) c-Si, (b) SiNSs and (c) a-Si displayed in the different circles	37

LIST OF TABLES

Table No.	Title	Page No.
4.1	Value of short range order D obtained from fitting of Raman spectra AS1 and AS2 from equation	20
4.2	Values of A and γ for silicon nanostructures shaped as sphere/column	35

ACRONYMS

Acronym	Meaning
NSs	Nanostructures
SiNWs	Silicon Nanowires
SiNSs	Silicon Nanostructures
PL	Photoluminescence
MIE	Metal Induced Etching
FE-SEM	Field Emission Scanning Electron Microscopy
PCM	Phonon Confinement Model
MPCM	Modified Phonon Confinement Model
FWHM	Full Width at Half Maximum
ZCP	Zone Centre Phonon
CB	Conduction Band
VB	Valance Band
c-Si	Crystalline Silicon
n-Si	Nano Silicon
a-Si	Amorphous Silicon

Chapter 1

Introduction

Nanotechnology deals with various structures of matter having dimensions of the order of billionth of a meter. While the word nanotechnology is relatively new, the existence of functional devices and structures of nanometer dimensions is not new, and in fact such structures have existed on earth as long as life itself. The first observation was that materials have been and can be nanostructured for new properties and novel performances. The underlying basis for this is that every property of material has a characteristic or critical length associated with it. For example, the resistance of a material that results from the conduction electrons being scattered out of the direction of flow by collision with vibrating atoms and impurities, can be characterized by a length called the scattering length. This length is the average distance an electron travels before being deflected. The manifestation of fundamental physics and chemistry changes when the dimensions of a solid become comparable to one or more of these characteristic lengths, many of which are in nanometer range. One of the most important examples of this is what happens when the size of a semiconducting material is in the order of the wavelength of the electrons or holes that carry current.

If only one length of a three dimensional nanostructure is of nano dimension, the structure is known as quantum well, the electronic structure is quite different from the arrangement where two sides are of nanometer length, constituting what is referred to as a quantum wire. A quantum dot has all three dimensions in the Nano range. The changes in electronic properties with size result in major change in optical properties of Nano sized material, along with the effects of reduced size on the vibrational properties of materials.

Semiconductor nanowires are of great interest due to their potential in electronic, optoelectronics, and sensor applications. Silicon nanowires (SiNWs) have received the most attention due to historical role of silicon in the integrated circuits(IC)[1] industry. Continued high performance from silicon may require alternatives to thin film planar CMOS transistors in the form of novel devices[2], three-dimensional structures, innovative architectures, and integration with other functional components. SiNWs may provide new avenues in these directions. Silicon becomes a direct band gap semiconductor at nanoscale dimensions and thus may have interesting optoelectronics applications[3,4]. Quantum size effect in nanowires will have an impact on electronics[5] and photonics [4,6,7]applications. Quantum confinement occurs when the nanomaterial dimensions approach the size of an exciton in bulk crystal[8], called the exciton Bohr radius. This lead to an increase in band gap with a decrease in size[9,10] of the nanomaterial.

One approach to the preparation of nanostructures, called the bottom-up approach, is to collect, consolidate, and fashion individual atoms and molecules into the structure. This is carried out by a sequence of chemical reactions controlled by catalyst.. The opposite approach to the preparation of nanostructures is called the top-down method, which starts with a large-scale object or pattern and gradually reduces its dimensions or dimensions. This can be accomplished by a technique called lithography which shines radiation through a template on to a surface coated with a radiation-sensitive resist; the resist is then removed and the surface is chemically treated to produce the nanostructure.

The fabrication of semiconductor nanowire falls in the category of top-down approach[11] .The fabricated nanowires are then characterized using one of the best spectroscopy tools called Raman Scattering[12]. In order to extrapolate the hidden physical phenomena and process that takes place in

the confined regime, it is very important to deeply analyze the theoretical Raman line shape obtained from various proposed models. Only then, one can find out various interaction line Fano[13,14] , effect of doping[15], stress[16], on the confined system. Various characteristics obtained from the Raman spectra of nanocrystalline silicon like FWHM (Full Width at Half Maximum), asymmetry ratio (deviation from symmetry), and the Raman shift which are different from the bulk spectra (Raman spectra of bulk silicon is sharp and symmetric centered at 520cm^{-1}) corresponding to ZCP[17].

So, far the theoretical models for c-Si and n-Si silicon have been proposed and widely studied. But for a-Si none of such model has been proposed to explain the physics lying in the spectrum. Mostly a Gaussian fit is used to deconvolute the Raman spectra but it is unable to speak the physics lying under the envelope [18]. One of the models known as MPCM(modified phonon confinement model)[19] is employed here in order to explain the line shape from amorphous silicon due to its ability to explain the amorphous nature of Silicon when the dimensions of the material is reduced below its Bohr exciton radius. Along with this a widely used Bond Polarizability Model is also studied which calculates the Raman intensity by calculating Polarizability from each bond. This model though does not explain the asymmetry induced from the confinement but explains the Raman shift in a very proper manner. Also this model explains the dependence of Size with the Raman Shift appropriately in case of column and sphere[20]. This model is used to find out the short range order in amorphous silicon .To confirm the size The MPCM is also incorporated and hence the short range order is confirmed by using a twofold approach.

Chapter 2

Theoretical Background

2.1 Silicon and its Structure

As discussed earlier semiconducting nanowires are of great interest due to their potential in electronics, optoelectronics, and sensor applications. Above all Silicon nanowires have received utmost importance due to its historical role of silicon in the integrated circuits industry. Confining the dimensions of the bulk Silicon to tailor its optical, electronic, thermal and other properties in an improved manner has revolutionized the entire world in terms of nano sized device which are being used in every giant machines. Here various changes in properties of silicon due to its confinement has been explained. Silicon, at about 28%, is the second most abundant element in the Earth's crust after oxygen, and is mainly found in the silica or silicate forms, SiO_2 and SiO_4 respectively. It is a major constituent of nearly all rocks, the principal exceptions being pure limestone and evaporates. Considering the abundance of Silicon, it is the most used material in electronic devices.

Silicon in its purest form is an intrinsic semiconductor. Though its conductivity can be increased by mixing a suitable impurity in it[21]. The crystalline Si has same structure as diamond as two interpenetrating face-centered cubic primitive lattices as shown in Fig.2.1. The lattice constant of silicon is 0.357 nm

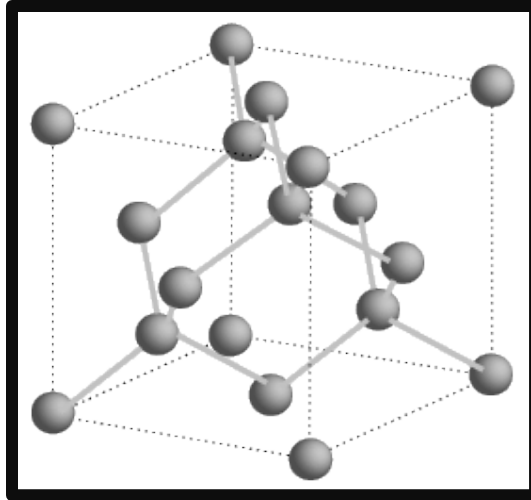


Figure 2.1 Silicon crystal structure

2.2 Band diagram of silicon:-

The k -vector for the electrons in a crystal is limited to a space called the Brillouin zone. The figure shows the Brillouin zone for the fcc lattice relevant for most semiconductors. The values and notations of certain important k -points are also shown.

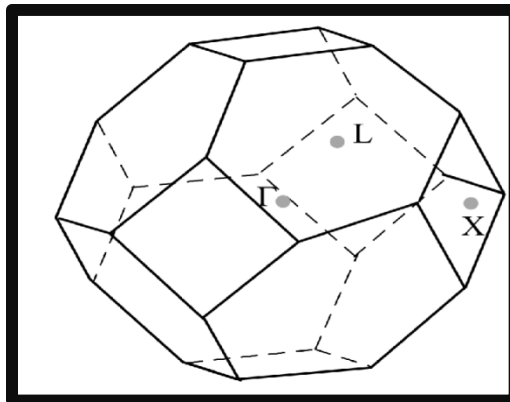


Figure 2.2 The values and notations of certain important k -points

Most semiconductors have band edges of allowed bands at one of these points. Bandgap plays a vital role in determining the optical properties of material. Figure 2.2 shows the energy band structure for crystalline silicon [33]. The symbols Γ , L, X, U and K are on the horizontal (wave vector) axis of the band structure plot representing different symmetry points in 3D k -space. Γ corresponds to $k=0$, the origin of Brillouin zone; Γ -X represents a path through Brillouin zone from centre to edge along the 100 direction; Γ -L and Γ -K represents middle to edge paths along the $\langle 111 \rangle$ and $\langle 110 \rangle$ directions. X-U represents path along the Brillouin zone boundary starting from zone edge on the $\langle 100 \rangle$ axis and moving in direction parallel to $\langle 101 \rangle$. A typical band diagram of silicon is shown in figure below.

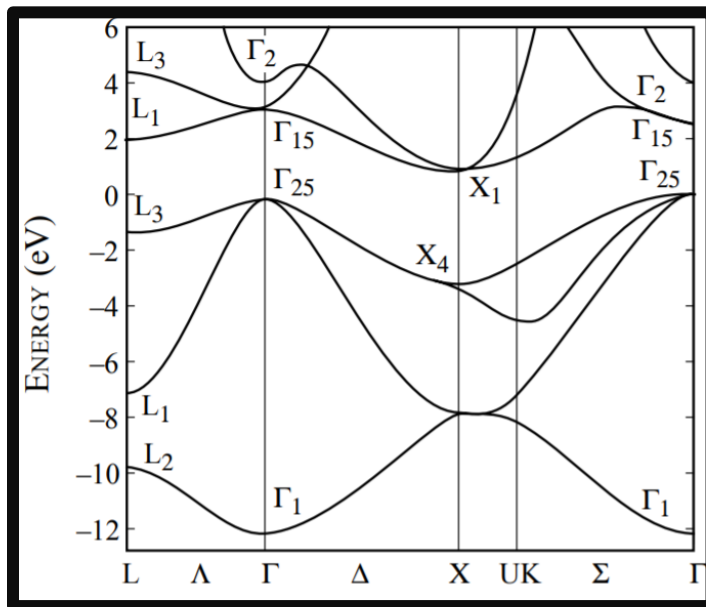


Figure 2.3 A typical band structure: Si

In c-Si, valance band maximum is located at centre of Brillouin zone (Γ point) and conduction band minimum is located at the X point along 100 direction (Δ) making it an indirect band gap material with band gap of

1.1eV. Therefore, c-Si does not show optical properties unlike GaAs, InP due to absence of radiative recombination.

Though Silicon is non-toxic, relatively inexpensive, easy to process, and has good mechanical properties but still due to its inefficiency in emitting light, bulk Si is not ideal for use in optoelectronic applications. The reason behind its inability to use for optoelectronic applications is its indirect energy band gap. Indirect energy bandgap in a semiconductor means, the maximum of the valence band and the minimum of the conduction band do not occur in the same value of k in the k -space. In an indirect semiconductor momentum conservation does not allow the recombination by a single photon which possesses negligible momentum. Therefore, momentum conservation takes place via phonon. Light emission efficiency is very less in bulk because non radiative process dominates over the phonon assisted optical transition. Bulk silicon is therefore not suitable for the fabrication of optoelectronic devices.

2.2.1 Effect of quantum confinement

When the size of the crystallite approaches its Bohr exciton radius, then materials show quantum confinement effect. The optical[7], electronic[15], magnetic and various other properties change due to this confinement. Considering Si as the material when reduced in its dimensions from the bulk form, it becomes a direct band gap semiconductor[22], this happens due to the fact that as the size of the material is reduced, the band structures become more flat as compared to its bulk form. Also Si in its bulk form does not show PL. But when its size is reduced it gives a PL[23] due to the breaking of $\vec{q} = 0$ selection rule. The possible explanation for it is the uncertainty principle $\Delta q \cdot \Delta x = 0$. So when the size of the crystalline is very large the only possible way remaining for the electron is to conserve the wave vector and hence only transitions with $\Delta q = 0$ are allowed (hence only direct transitions possible) but as the

uncertainty in the movement of electron in the nano-crystallite is of the order of D , so all the possible transitions of the order of wave vector $1/D$ are possible in case of n-Si. The effect of Quantum confinement on the Raman scattering of SiNSs is worth analyzing because a lot of information about the physical process can be derived, which are taking place at the nanoscale. The Raman spectra of Bulk silicon corresponds to a sharp symmetric line shape centered at 520 cm^{-1} attributed to the fact that only ZCP participate in scattering process. But as the size is gradually reduced to nano dimensions then the Raman spectra acquires a Red shift and a broadening which depends on the size of the nano-structures. Various key parameters like FWHM (Full Width at Half Maximum), asymmetry ratio delivers a lot of information about the perturbation induce in the system.

Chapter 3

Experimental Techniques

This chapter explains the characterization methods that are used for the samples prepared. All the techniques used are explained in detail.

3.1 Field emission scanning electron microscope (FESEM)

The Scanning Electron Microscope gives surface morphology, topology, and structural composition of material. It is an electron microscope that works on the principle of scanning the images of the sample with a high energy electron beam. It is different than the optical microscope in a sense that optical microscope use series of glass lenses to bend light waves and create an image while this uses electron beam and then creates a magnified image.

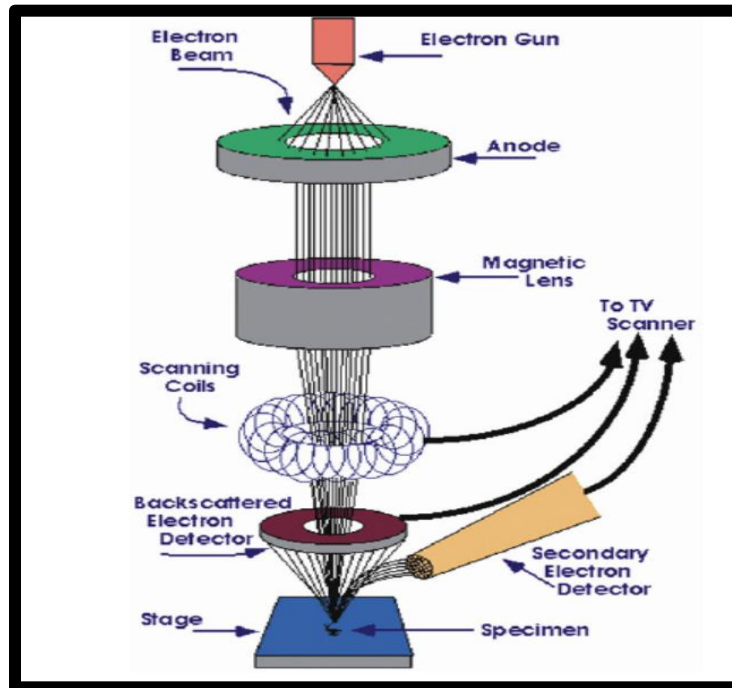


Figure 3.1 Schematic diagram of FESEM

When the beam of electron interacts with the sample. Due to this interaction, different types of electrons are also generated called as secondary electrons (SEs), backscattered electrons (BSEs), auger electrons, X-rays, etc. In this work FESEM images were recorded using Supra T M 55; Carl Zeiss.

3.1.1 Types of Signals generated:

As explained that above that different types of electrons generated give rise to varied signals and information regarding the sample. But primarily used signals are generated using secondary and backscattered electrons which are explained below

i) Secondary electrons

As the incident electron beam enters the specimen and hits the constituent atoms in the specimen, the valence electron from the atoms are emitted depending on the energy of the electron beam. These electrons generated at the top surface are emitted outside of the specimen. As these originate from the near surface or near surface regions of the sample, secondary electrons are used to analyze the topography of the specimen. Also, the yield of the secondary electrons depends on the accelerating voltage of the electron beam. The energy of these electrons is usually less than 50eV.

ii) Backscattered electrons

These are sometimes called reflects electrons, as these are the electrons that are reflects back by the specimen due to repulsion between the electron beam and the electrons of the specimen. These electrons have higher energy than the Secondary electrons so they deliver information from a relatively deep region of the specimen. As these electron depends on the coulomb repulsion so these are helpful in differentiating among different components in the specimen. So, if

the backscattered yield from an area of the sample is larger than the other then that means it has atoms with relatively higher atomic number. So, an area that consists of a heavy atom will appear bright in the imaging.

3.1.2 Instrumentation

Major components in an SEM involve the electron gun, which is on the top of the column which is used to produce electrons and accelerate them to an energy level of 0.1-30 keV. Electromagnetic lenses and aperture are used to focus and define the electron beam. Also the specimen stage, signal detection system and image recorder is required.

i) Electron source

It produces an electron beam using an thermionic emission gun emitted by heating the tungsten filament at very high temperatures. These thermo electrons are gathered as an electron beam, flowing into a metal plate by applying a positive voltage. The illumination system of FESEM consists of an electron source, which is maintained at a negative potential. The emitted electron beam, which typically has an energy ranging from a few hundred eV to 30 KeV, is passed through a magnetic lens system.

ii) Lenses (Condenser lens and objective lens)

The lenses are used to collimate the energetic electron beam from the electron gun. Combining the lenses and the electron gun probe is formed. An aperture is placed between the condenser and objective lens. The electron beam is allowed to pass through the aperture. The electron beam which passes through the condenser lens, illuminates this aperture plate. Depending on the excitation of the condenser lens. The objective lens is used for focusing and it determines the diameter of the electron beam

iii) Detector, Image Display and Recording:

A fluorescent substance is used to coat the tip of the detector by using a high voltage of about 10 kV. The electrons get attracted to this voltage and then produce scintillation when they hit the fluorescent. By using a Photomultiplier tube this light is enhanced. This enhanced light is converted to electrons, and these electrons are amplified as an electric signal. The output signals from the electron detector are amplified and then transferred to the display unit synchronized with the electron probe scan.

3.2 Raman Spectrometer:

As explained earlier that Raman spectroscopy is a very compatible tool to find structural composition, optical properties. It is a kind of inelastic scattering which occurs when the photon of a particular frequency falls on the material. When light is scattered from a molecule or crystal, most photons are elastically scattered. The scattered photons have the same energy (frequency) and, therefore, wavelength, as the incident photons. However, a small fraction of light (approximately 1 in 10⁷ photons) is scattered at optical frequencies different from, and usually lower than, the frequency of the incident photons. The process leading to this inelastic scatter is termed the Raman Effect. Raman scattering can occur with a change in vibrational, rotational or electronic energy of a molecule. If the scattering is elastic, the process is called Rayleigh scattering. If it's not elastic, the process is called Raman scattering. Different detection parts in the spectrometer are (a) source, (b) spectrometer and (c) detection/recording unit, are shown schematically in the figure. 3.2. An argon-ion laser (Coherent INNOVA 90-5 model) was used as an excitation source for Raman scattering experiments while for detection of signals

Charged Couple Devices (CCD) are used because of their sensitivity to light which makes them suitable for inherently weak Raman signal analysis.

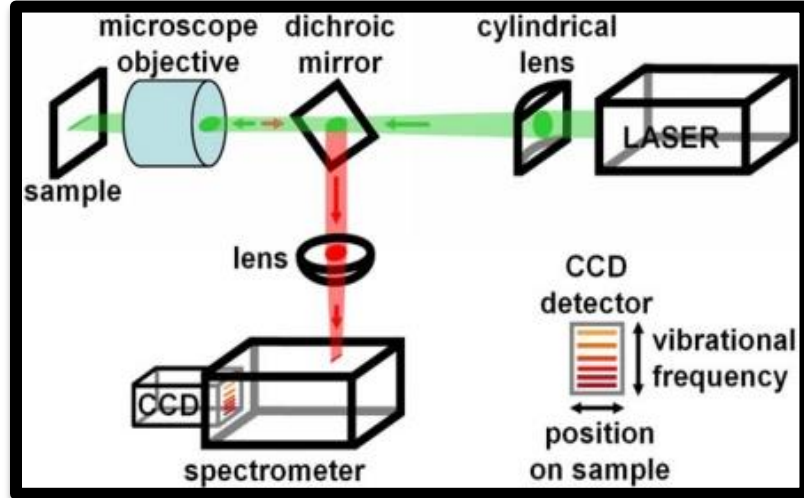


Figure 3.2 Schematic diagram Raman Spectrometer.

3.3 Sample Preparation

3.3.1 Method used for preparation

Metal induced etching (MIE) method is adopted for fabricating SiNWs. Amongst various methods used for fabrication of pSi/SiNSs [23–26] , MIE is one of the simplest and economical methods for synthesis of semiconductor NSs . The steps involved in sample preparation are discussed below.

i) Substrate cutting and cleaning

Silicon wafers of required dimensions were cut using a diamond tip glass cutter. Cleaning of substrates is critical for sample fabrication by MIE; these were cleaned to remove inorganic. Substrates were subsequently cleaned in acetone and iso-propanol solutions for 10 minutes each.

ii) Surface treatment

Substrates were further washed with 5% HF solution to remove the thin oxide layer that is formed on the surface of silicon wafer due to exposure to air and then with distilled water to remove excessive fluoride ions.

iii) Metal nanoparticle deposition

These wafers were then dipped in solution containing 4.8M HF and 5mM AgNO₃ for required deposition time to deposit Ag NPs and then rinsed with distilled water to remove extra silver ions. This step is crucial to determine the diameter of SiNWs.

iv) Etching process

The Ag NPs deposited samples were then kept for etching in an etching solution containing 4.6 M HF and 0.5 M H₂O₂ according to desire. Etching time decides the length of the SiNWs. This step is also known as porosification time.

v) Removal of Ag particles after porosification

Etched wafers were transferred to HNO₃ to remove Ag NPs after the etching process. Then the samples were dipped into HF solution to remove oxide layer induced by HNO₃ used in above step.

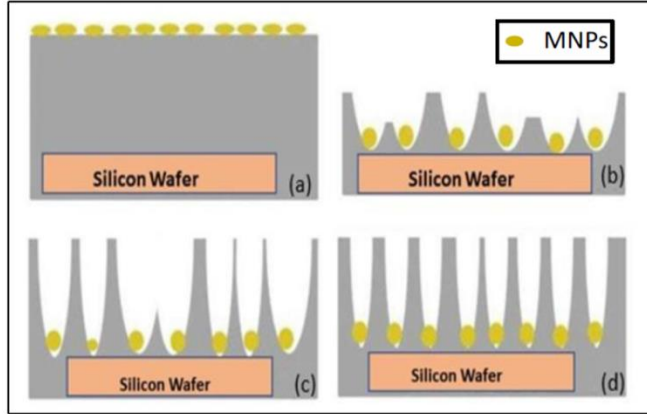


Figure 3.3 Block diagram of MIE mechanism. (a) Ag nanoparticle coated Si wafer. (b), (c) and (d) etching in HF + H₂O₂ solution

3.4 Metal Induce Etching Mechanism

MIE mechanism is very simple and popular method to fabricate Semiconductor NSs . As already mentioned in chapter 3 the MIE involves mainly two steps, (i) deposition of MNPs on a clean Si wafer and (ii) etching of this metal deposited wafer in an etching solution consisting of HF and H₂O₂. In the present study, AgNPs have been used, which is deposited on Si wafer by dipping a clean Si wafer into a solution of AgNO₃ and HF. Ag⁺ ions, available in this solution, when come in contact with Si surface, accept one electron from the Si and get neutralized as AgNPs.

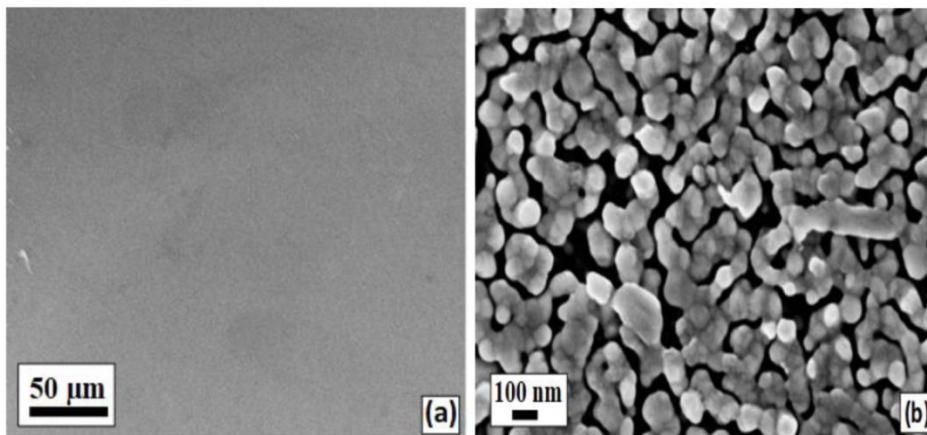


Figure 3.4 (a) Ag nanoparticle coated Si wafer. (b) Ag NPs deposited on silicon wafer

The transfer of electron from Si to Ag^+ is favorable because the redox energy for the pair Ag^+/Ag (0.79 V) is higher than the valence band energy of Si (0.62 V) [8]. This transfer of electron from Si to Ag^+ results the injection of hole (h^+) (creation of positive site in Si) in the Si. The injection of hole inside the Si is necessary to start the porosification [3, 9–11] using HF acid. These AgNPs deposited Si wafers are put into the etching solution of HF and H_2O_2 where the positive sites of Si, created in the previous step, gets attacked by fluoride ion (F^-). This forms H_2SiF_6 before getting dissolved in HF solution and creates a pit on the Si surface. Further, transfer of another electron from Ag to H_2O_2 takes place which results in reduction of H_2O_2 and creation of Ag^+ to start next cycle of etching by providing continuous supply of Ag^+ and thus of h^+ . For this process, transfer of electron is favorable because the redox energy for the pair $\text{H}_2\text{O}_2/\text{H}_2\text{O}$ (1.78 V) is higher than the redox energy for the pair Ag^+/Ag (0.79 V). In this way the AgNPs penetrate deeper into the wafer as porosification proceeds. The etching time (continuation of cycle) decides the depth of pits in the Si.

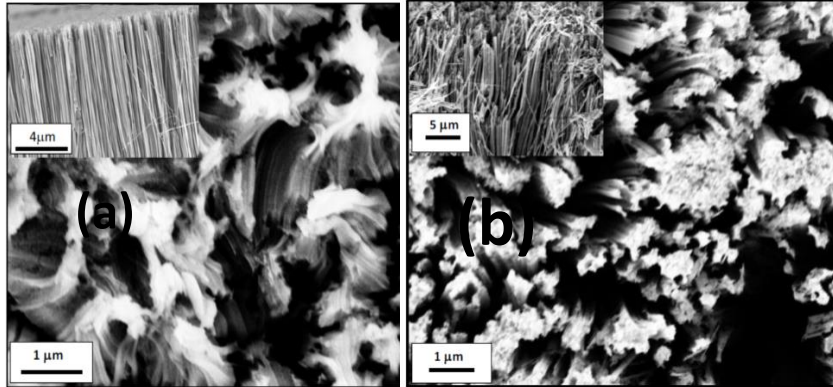
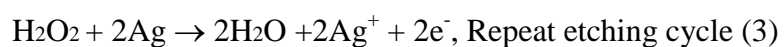
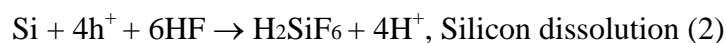


Figure 3.5 (a) Surface morphology of etched Si surface and cross-sectional view (insight) of AgN01 (b) Surface morphology of etched Si surface and cross-sectional view (insight) of AgP01

which is dictated step by step in details as follows: (1). Ag^+ ion available in solution, sits on Si wafer takes one electron from Si wafer and create positive site in Si. (2) F-ions available in solution of HF and H_2O_2 , attacks on the positive sites of Si. (3) As a result of reaction between F-ion and Si at the positive sites, H_2SiF_6 formed. In this way Si atoms get out from Si wafer and result pit in Si wafer. (4) To repeat the above process (step 1 to step 3), H_2O_2 takes one electron from Ag to form Ag^+ . This process repeated again and again which decides the depth of pits and can be controlled by the etching time (time of living of AgNPs deposited Si wafer in etching solution). (5) Finally after the particular etching time, the AgNPs are removed by the dipping that wafers in HNO_3 and obtained SiNWs on Si wafer.

The chemical reactions involved in fabrication of Si NSs using porosification by MIE are:



Chapter 4

Results and Discussions

4.1 Phonon Confinement Models

In the present work, an attempt has been made to prepare and understand a theoretical model which explains the quantum confinement effect in a more precise manner. The Raman spectra of bulk c-Si, exhibits a symmetric peak at 520 cm^{-1} , due to optical phonon dispersion curves, with a line width(FWHM) Γ (3 cm^{-1})[27]. In nanocrystals, valuable experimental information can be obtained by Raman spectroscopy, as a function of size, through the energy shift of the Raman peak and correspondent line broadening, both size dependent.

The classical theory of radiation from an oscillating dipole demonstrates that Raman peaks have lorentzian shape[28] given by the equation

$$I(\vec{\nu}) = I_0 \int \frac{d^3k}{[\vec{\nu} - \nu(k)]^2 + \left(\frac{\Gamma}{2}\right)^2} \quad (4.1)$$

The scattering of one photon ($\vec{k} = 0$) by n phonons (k_i) is governed by momentum conservation rule.

$$\sum_{i=1}^n \vec{k}_i = \vec{k}_{scattered} - \vec{k}_{incident} = \vec{0} \quad (4.2)$$

Therefore only vibrations from the Centre of the BZ can be active in any one phonon process.

In a finite size crystal, the translational symmetry of lattice is no longer conserved due to the presence of the grain boundaries that result in confinement of phonons, and triggers a red shift of the characteristic phonon mode with decreasing size. To explain the confinement, various phonon confinement models have been deployed in the above equation suitably.

The Raman line shape from n-Si is asymmetrically broadened and has a red shift as compared to its bulk counterpart[29]. In order to understand Raman spectra from n-Si, various models that have been proposed are.

i. Bond Polarizability Model(BPM)

To explain the vibrational properties of n- Si, the bond polarizability model is used extensively. It is found that this model can give a good description of the scattering intensity from optical modes. In this model, the polarizability of the whole system is calculated as a sum of independent contributions from each bond, Based on the calculated eigen values and eigen vector. The variation of the $\mu\nu$ component of the polarizability tensor due to phonon mode j with wave vector $\mathbf{q} \sim 0$ is a sum of the contributions from each bond in the whole system[19,20], given as

$$\Delta\alpha_{\mu\nu}(\mathbf{j}\mathbf{q}) = \sum_i^{bonds} \Delta\alpha_{\mu\nu}(i\mathbf{j}\mathbf{q}) \quad (4.3)$$

Where $\Delta\alpha_{\mu\nu}(i\mathbf{j}\mathbf{q})$ is the differential polarizability of the ii^{th} bond in the system considered. Then the Raman-intensity in the $\mu\nu$ polarization for the backscattering configuration is given by

$$I_{\mu\nu}(\omega)\alpha[n(\omega) + 1] \sum_j \delta(\omega - \omega_j(\mathbf{q})) |\Delta\alpha_{\mu\nu}(\mathbf{j}\mathbf{q})|^2 \quad (4.4)$$

Here $[n(\omega) + 1]$ is the Bose-Einstein population factor.

$$\text{The Raman shift is given by } \Delta\omega = \omega(L) - \omega_0 = A \left(\frac{a}{D}\right)^\gamma \quad (4.4(a))$$

Here A and γ are fitting parameters, a is the lattice parameter for silicon unit cell (0.357 nm) and D is the diameter of the nanowire.

Though this model explains the Raman-shift acquired by nanocrystals due to confinement but is unable to explain the asymmetric red shifted broadening, which is a prominent signature of confinement. The above mentioned flaws have been rectified by incorporating various confinement functions in the Raman line shape equation for bulk c- Si. A figure of Raman shift vs size has been shown below using the relation given between shift and size of the nanostructured column and spheres. It is clear from the figure that the shift is significant as the size of the

nanostructure is decreased. This work published by Xian Ji *et al.* was done using partial density calculations.

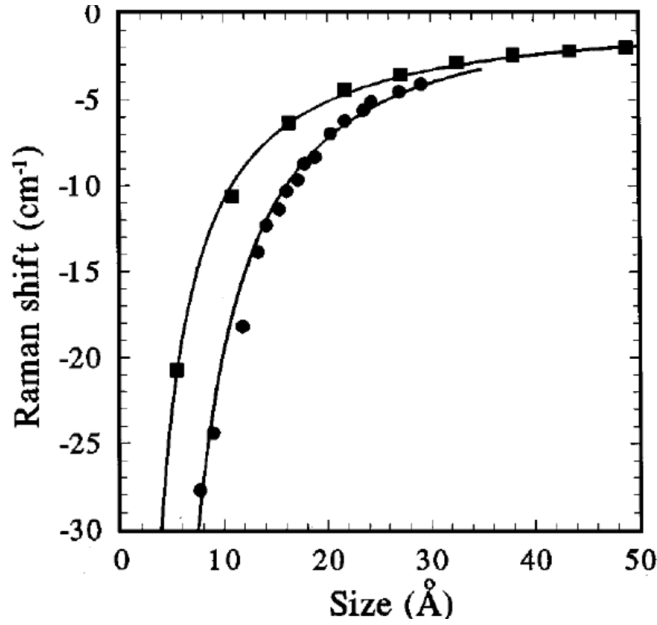


Figure 4.1 Raman shifts vs. size for Si spheres and columns (Zi J. *et al.*)

	A(cm ⁻¹)	γ
Sphere	47.41	1.44
Column	20.92	1.08

Table 4.1: Values of A and γ for silicon nanostructures shaped as sphere/column

ii. Phonon Confinement Model (Sinusoidal weighting function)

To understand the size effect on Raman line shape of semiconductors NSs, a spherical crystal with diameter D is assumed such that the phonon is confined in the volume of the crystallite[30,31]

Wave function of the phonon is given as

$$\Psi(\vec{q}, r) = F_C(r, D)\phi(\vec{q}, r) = \Psi'(\vec{q}, r)u(\vec{q}, r) \quad (4.5)$$

Where $u(\vec{q}, r)$ has the periodicity of the lattice and $F_C(r, D)$ is the phonon weighting function which can be Fourier transformed as

$$F_C(r, D) = \int C(\vec{q})\exp(i\vec{q}.r)d\vec{q} \quad (4.6)$$

Therefore, the first order Raman spectrum of a nanocrystal can be calculated as:

$$I(\omega) \propto \int \frac{|C(\vec{q})|^2}{[\omega - \omega(q)]^2 + \left(\frac{\gamma}{2}\right)^2} d\vec{q} \quad (4.7)$$

Where $\omega(q)$ is the phonon dispersion relation curve and γ is the natural line width ($\gamma = 3 \text{ cm}^{-1}$).

The selection of phonon confinement function and choosing a proper dispersion relation plays a key role in the Raman analysis. Considering the fact that the $\vec{q} = 0$ selection rule breaks due to confinement and phonon vector other than the zone centre also participates in the Raman scattering. So, this model considers phonon as a wave function in a dot as a weighted superposition of sinusoidal waves[19,30,32] with

$$k_n = n\pi/D, \quad n = 2, 4, 6 \dots n_{max}:$$

$$F_C(r, D) = \sum_n \frac{\sin(k_n r)}{k_n r}, \quad \text{for } r \leq D/2, \text{ or } 0 \text{ otherwise. Using this, the one}$$

dimensional Fourier Transform of $F_C(r, D)$ is given by

$$C_n(q) = 3 \frac{\sin\left(\frac{qD}{2}\right)}{\pi^3 D^3 q \{k_n^2 - q^2\}}$$

The Raman spectrum is given by :

$$I(\omega) \propto \int_{2\pi-1}^{2\pi+1} \frac{4\pi Q^2 \left| 3 \frac{\sin \frac{Q}{2}}{\pi^3 Q \{4\pi^2 - Q^2\}} \right|^2 \left(\frac{\gamma}{2}\right)}{\left[\omega - 521 \left(1 - 0.23 \left(\frac{Q a_{si}}{2\pi D} \right)^2 \right) \right]^2 + \left(\frac{\gamma}{2}\right)^2} dQ \quad (4.8)$$

Where the dispersion relation used is given by

$$\omega(k) = 521 \left(1 - 0.23 \left(\frac{Q a_{si}}{2\pi D} \right)^2 \right).$$

The theoretical Raman line-shape is shown in the figure below

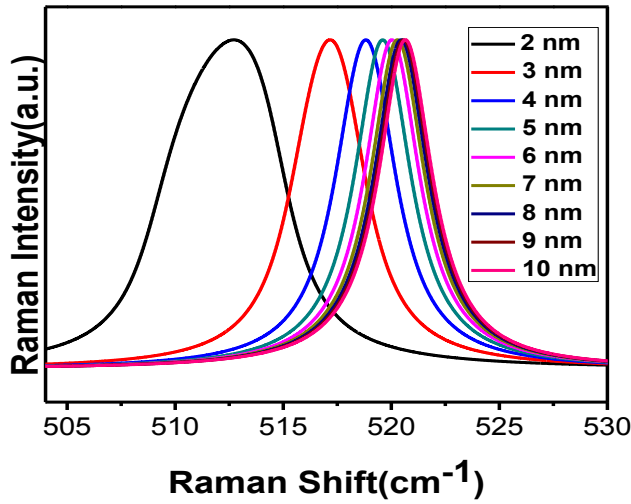


Figure 4.2 Raman shifts as a function of size obtained from MPCM

The justification for the choice of the wave function is given by:

- i. The phonons are of different wave vector for the nanocrystal, so a complete wave packet is considered instead of the single phonon.
- ii. The above wave function vanishes at the boundary of the nano dot, which is realistic due to the phonon confinement within the dot itself.

- iii. The wave vector of the phonon follows the Heisenberg uncertainty principle with a spread $\Delta r = D$ in real space and $\Delta q = 1/D$ in q space.

Considering the limits of the integration over the q wave vector and the dispersion relation, it is an elucidated conclusion that for a nanocrystal the limits of the integration selects a narrow region at lower energy with respect to the maximum. One important thing that needs to be highlighted is the limits of the integration are imposed keeping in mind the Heisenberg principle, which are indeed size dependent, which results into a large shifting when the confinement becomes strong. This model has been considered appropriate due to the choice of the limit which restricts the scattering process in the limits $\frac{[n\pi-1]}{D}$ to $\frac{[n\pi+1]}{D}$ due to the momentum conservation[32]. Though this model has a sound explanation of theories and explains the Raman shift in a vivid manner. But is still not able to give a relatable and exact description of the asymmetry in the Raman line-shape which arises due to confinement and is also one of the key features which describe the quantum phenomena of confinement.

iii. Phonon Confinement Model (Exponential weighting function)

By far, it is worth mentioning that the choice of the weighing function plays an important role in explaining various physical phenomena, size, and phonon participation in the semiconducting nanowire. The key features that helps in explaining is the asymmetric broadening accomplished by a red shift depending on the size of the nanowire. A lot of information can be extracted from these features, because these features also depend on temperature, stress, electron-phonon interaction to which system is

subjected. Richter *et al.* [27] gave a theoretical model to elaborate the effect of confinement in SiNSs which was modified later by Cambell and Fauchet [33] to incorporate the changes in the raman line-shape. This model is still widely used due to its capability to explain the perturbation induced after the confinement. Writing wave vector q_0 in an infinite crystal as $\Phi(q_0, r) = u(q_0, r)e^{-iq_0 r}$, where $u(q_0, r)$ has the periodicity of the lattice, the phonon in a microcrystal of diameter become $\Psi(q_0, r) = W(r, L)\Phi(q_0, r) = \Psi(q_0, r)u(q_0, r)$ where $W(r, L)$ is the phonon weighting function. Richter et al. chose $W(r, L)$ to be Gaussian.

So, the Fourier transform is given as

$$F_c(r, D) = e^{-\frac{q^2 D^2}{4a^2}}$$

And the Raman line-shape equation for the scattering is given by.

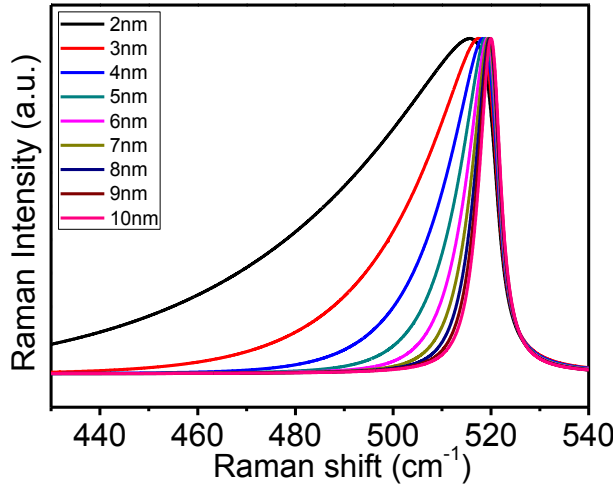


Figure4.3 Raman spectra simulated from PCM equation

$$I(\omega) \propto \int_0^1 \frac{e^{-\frac{q^2 D^2}{4a^2}}}{[\omega - \omega(k)]^2 + \left(\frac{\gamma}{2}\right)^2} d^n k \quad (4.9)$$

Here $\omega(k) = \sqrt{A + B \cos \frac{\pi k}{2}}$ is the optical dispersion relation used for Si. Where $A=171400 \text{ cm}^{-2}$ and $B = 100000 \text{ cm}^{-2}$. The degree of confinement used is d^2k because the nanostructures under study are SiNWs which are confined in two dimensions.

Due to the physics involved in the choice of the confinement function, this model explains all the significant perturbation involved in the Raman line-shape due to confinement. The Raman line shape obtained from the above theoretical model is shown as below

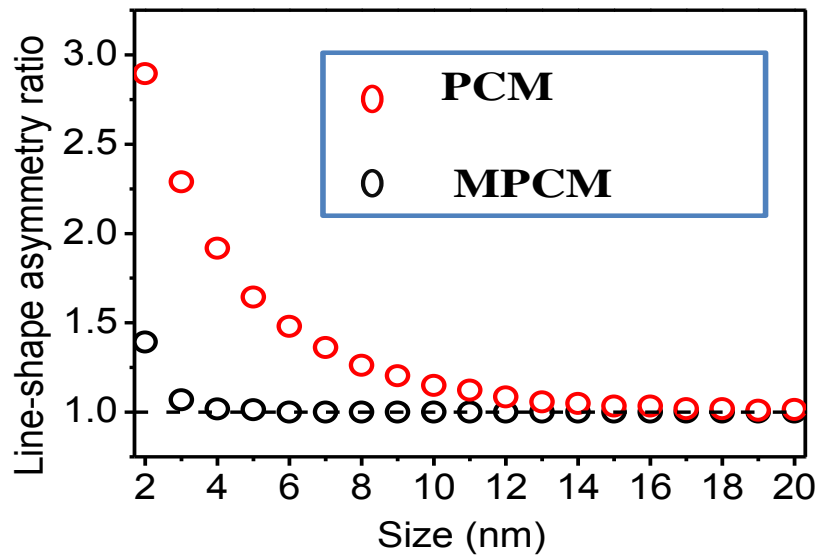


Figure 4.4 Asymmetry ratio vs size for MPCM and PCM

After analyzing the line shapes from nanostructured silicon, various parameters like FWHM, asymmetry ratio were also analyzed. The asymmetry ratio in case of MPCM remains almost unity after increasing the size from 2 nm while in case of PCM the asymmetry ratio increases as the size of the nanowire is decreased. Figure above explains it in more illustrative manner.

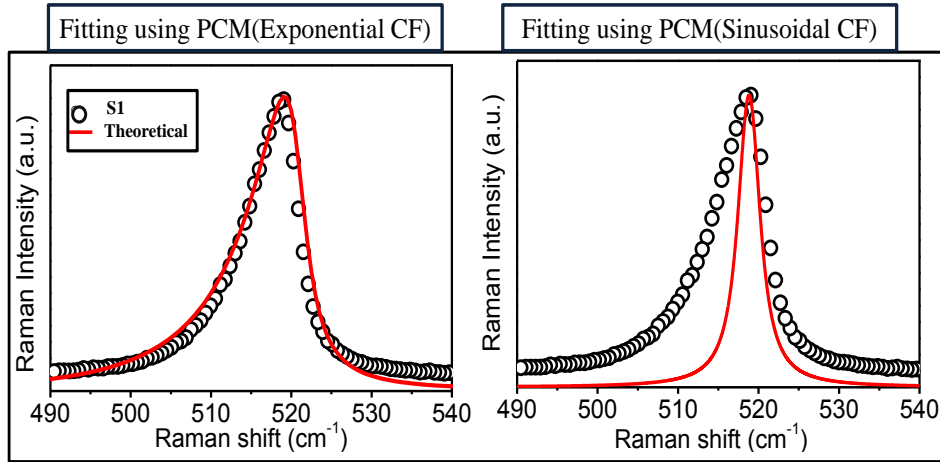


Figure 4.5 Fitting of experimentally observed Raman scattering data (discrete points) by using equation (4.8) and (4.9)

Raman fitting of fabricated nanowires was done using both the models (MPCM and PCM). Discrete points in Figure 4.5 shows the experimentally obtained data whereas the solid lines in red is the line-shapes generated using Eq. 4.8 and Eq. 4.9 respectively. As can be seen clearly from Figure, the experimental Raman data does not fit with the theoretically obtained line-shape when crystallite size of 7 nm is used in Eq. 4.8 (MPCM). In fact, we have also try to fit the Raman line-shape obtained using different sizes between 2nm-10 nm which also do not show fit with the experimental data. On the other hand, the experimental Raman scattering data shows a good agreement with the line-shape generated using Eq 4.9 (PCM) for a crystallite size of 7 nm as shown in red curve (Figure 4.5).

It is very clear from above discussion that the MPCM does not represent the actual Raman scattering phenomenon taking place from low dimensional SiNSs, whereas PCM still appears to be the more generalized form for representation of the Raman line-shapes[34]. The reasons for the incompleteness of Equation 4.8 include the non-consideration of the

participation of absolute zone-centre phonons in the Raman scattering from n-Si. Rather MPCM considers that the zone centre of the phonon dispersion gets shifted due to finite size similar to the shifting of the band edge as discussed in the context of size dependent band gap enhancement in nano-Si[35]. It is worth mentioning here that, considering the shift of the phonon dispersion zone centre all-together sounds a nice approach for explanation of Raman line-shapes at nanoscale but at the same time appears incomplete. Another possible advantage of using Equation 4.8 is the consideration of partial phonon dispersion curve to take care of the momentum conservation. This also, though conceptually correct, leads to the discrepancy between the Equation 4.8 and experimental Raman scattering data. A better way to consider the zone centre shift and momentum conservation needs to be explored but in the absence of it, PCM still seems the best and more generalized form of the Raman line-shape from n-Si.

4.2 Study of Raman Spectra from Crystalline, microcrystalline and amorphous Silicon

4.2.1 Raman Spectra from Crystalline Silicon:-

In c-Si, due to long translational symmetry in the crystal all the phonons that vibrate with a particular frequency take part in the Raman scattering. So, the Raman line shape shows a sharp peak at 520 cm^{-1} corresponding to the zone centers phonons. Considering the optical dispersion relation, in Raman scattering from crystalline silicon, phonon only at the Brillouin zone center take part. This is due to the $\vec{q} = 0$ selection rule conservation. There is a well-established theoretical model to explain the intensity from the Raman scattering given by the symmetrical lorentzian line-shape given by the equation:

$$I(\omega) \propto \frac{1}{[\omega - \omega_0]^2 + \left(\frac{\gamma}{2}\right)^2} dk \quad (4.10)$$

Where $\omega_0 = 520 \text{ cm}^{-1}$ corresponds to the Brillouin ZCP. Figure below shows the Raman line-shape from crystalline silicon

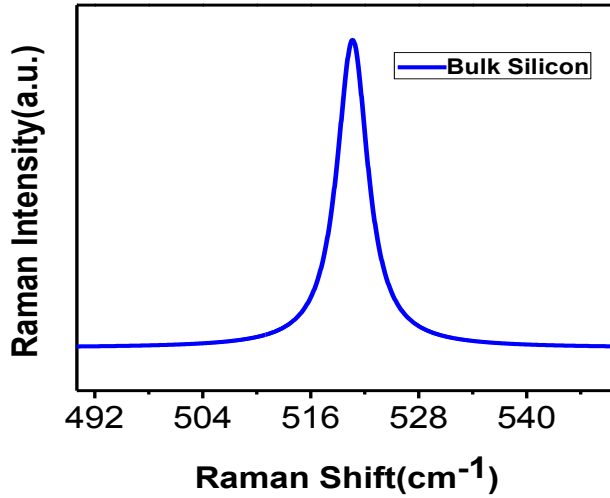


Figure 4.6 Raman spectra for c-silicon (bulk)

4.2.2 Raman Spectra from Silicon nanostructures:-

As explained earlier the Raman scattering is a superior tool not only to study the structure, doping level and composition but also to peek into the various physical phenomena which takes place in semiconductor NSs. It gives an accurate idea about the size distribution by fairly evaluating the key features that appear in the Raman line shape of NSs. When the size of the material is in between the Bohr exciton radius and the bulk then the Raman line-shape is asymmetrically broadened accompanied by a Red shift. This happens due to the violation of the momentum conservation rule, i.e. as the dimensions of the material is reduced the $\vec{q} = 0$ selection rule is broken due to the breaking of the translational symmetry and

phonons other than the zone centered ones starts participating in the Raman scattering. The Raman line-shape is accompanied by a phonon confinement function which imposes the condition of restricting the movement of phonon in the nanocrystalline. The obtained Raman line shape is given by.

$$I(\omega) \propto \int \frac{|C(\vec{q})|^2}{[\omega - \omega(q)]^2 + \left(\frac{\gamma}{2}\right)^2} d\vec{q} \quad (4.11)$$

Where $C(\vec{q})$ is the confinement function. Depending upon the choice of the system the confinement function can be Gaussian, sinusoidal etc. A typical Raman line shape spectrum from nanowires of varied sizes is shown in the figure below.

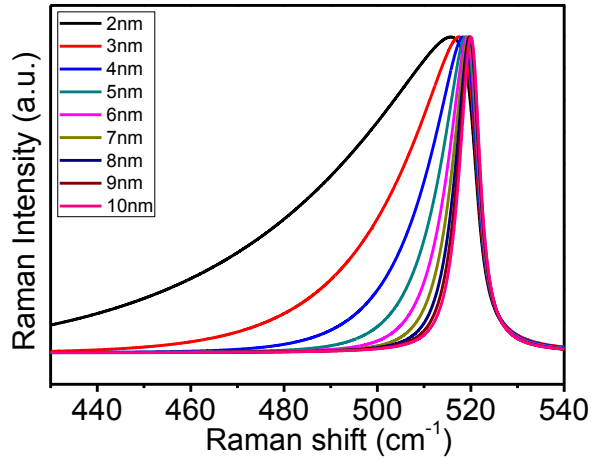


Figure 4.7 Raman spectra for different SiNWs size obtained from equation

4.2.3 Raman Spectra from amorphous Silicon:-

The Raman scattering from amorphous Silicon shows a broad peak ranging from $470\text{ cm}^{-1} - 485\text{ cm}^{-1}$ due to the breakdown of translational symmetry[36]. It happens because the order of crystallinity becomes really

short and is limited in each of the grain boundaries. Due to this the vibrational modes of the silicon has an influence from a density of the phonons instead of a single phonon as in the case of crystalline Silicon. So far there is no such theoretical model to explain the features of Raman line shape from a-Si. Also the variation of peak position in the different samples of amorphous silicon has some underlying physics which is not yet been explained properly. One of the most important aspects for a-Si is the study of its short range order. Because the use of a-Si in devices like Solar cell require the device efficiency to be maximum[37–39]. In order to maximize the efficiency there is an urgent need to study the various physics lying in Raman spectra of a-Si. There is no particular model to fit the Raman line shape from amorphous silicon. Usually it is fitted using Gaussian line-shape which has no underlying physics behind it. So, in the subsequent discussion a model has been explained giving a legitimate explanation of its use for fitting the Raman spectra of amorphous silicon. Also, a well-established model called BPM is also used to find out the size of the short range present in the amorphous silicon. Figure below explains the Raman scattering in c-Si, n-Si, and a- Si. As it is clear from the diagram that the Raman scattering in case of c-Si takes place via a single phonon process whereas in case of nanocrystalline and amorphous silicon a particular range of phonons and random phonons takes part respectively, due to the breaking of selection rules in both of these cases .Further as shown in case of nanocrystalline silicon a an integral is considered for adding up the continuous range of phonon, whereas in case of a-silicon there is no such pattern for phonon participation and phonons randomly participate .Thus the collective addition is shown as the discrete summation instead of continuous summation(integral).

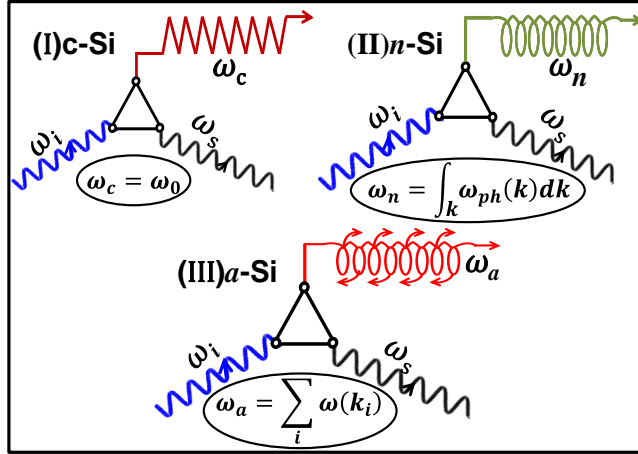


Figure 4.8 Illustration for depicting various Raman processes involving the scattering from c-Si, n-Si and a-Si.

4.2.4 Estimation of short Range order in amorphous silicon using Raman scattering:-

The increased demand of nanotechnology in Silicon solar cells requires a proper attention to study the theoretical approach which can lead to the maximization of the efficiency of the solar cells[40]. The size distribution in amorphous silicon has not been yet studied in a broad manner .Hence there is an urgent need to study and hence predict a model which suitably explains all the key parameters appearing in the Raman spectra of a-Silicon. In this section an attempt has been made to exploit short ranged ordering in amorphous Silicon[41,42] using MPCM and BPM. So far there is no detailed theoretical model to explain the broad Raman line shape arising from a-Si and to calculate the ordering in the hazy(amorphous like) system. So Raman scattering has been incorporated to study this physical quantity. As discussed earlier the Raman spectroscopy has already been widely exploited to study the optical properties of Bulk Silicon. Also one can easily study the effect of confinement on the bulk Silicon by analyzing the theoretical established models. Many studies have been done to

analyze the effect of temperature, pressure, high doping in the nanostructures[28] silicon using Raman spectroscopy. But the mystery of a-Si in many aspects remains unsolved. In an attempt to understand the underlying physics in the Raman spectrum of amorphous Silicon two widely used models have been revisited thoroughly and based on that various results regarding the short range order and the broadening in the spectrum has been explained properly.

As explained earlier that the MPCM fails to explain the asymmetry induced in the Raman line-shape of nanostructured Silicon due to the unit asymmetry ratio for sizes ranging from 2 to 15 nm. One of the reasons could be the changing dispersion relation for each size taken into consideration and also the limits of the q wave vector which are size dependent so every time the dispersion relation of the Silicon selects a different window for calculating the Raman spectra. On the other hand the Raman shift which is one key features of the confinement is properly incorporated by this model. It is because the shape of the TO optical phonon dispersion relation in silicon, which has its maximum at $\vec{q} = 0$, the Raman peak is at its maximum value (521 cm^{-1}) for a large crystal. But for a nanocrystal, the integration limits select a narrow region at lower energy with respect to the maximum, according to the limitations imposed by the Heisenberg relations, which are size dependent. This determines the shift. So all in all it does not serve the desire of confined phonons but the stimulated Raman spectra shows a-Si behavior when the size approaches towards Bohr exciton radius of Silicon. So, the MPCM is used to explain and fit the Raman spectra obtained from a-Si. The usual Raman spectra from a-Si is broad and shows a peak in the range $470 \text{ cm}^{-1} - 485 \text{ cm}^{-1}$. The experimental data when fitted from MPCM gives a value of D which is nothing but the short range order of crystallinity in a-Si. The Raman spectra is used to explain the vibration of phonon confined within the nanocrystal, similarly in amorphous silicon, all the vibrations are limited

to a the particular grain boundary which is short ranged. So the estimated size from Raman spectra from a-Si is nothing but the value in which one grain is located having same order of planes. This order comes out to be in angstroms. Amorphous silicon solar cells require the device efficiency to be maximum, this requires the size of the nanostructures to be desirable. For this the need of the hour is to put forward a theoretical model which quantifies the short range order present in the amorphous silicon. So, data from various authors have been taken and the short range order present has been quantified.

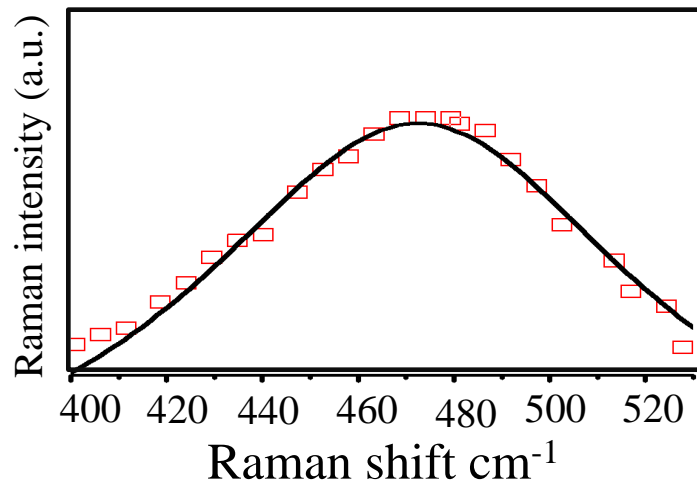


Figure 4.9 Raman spectra of a-Si of samples AS1, discrete data points show the experimentally obtained Raman spectra whereas solid line corresponds to theoretical fitting (Eq. 4.8).

The size that has been estimated from the fitting is depicted in the table 4.2. Looking at the fitted spectra of various data, it appears that the fitting has succeeded in exploring the short range order in amorphous silicon. But mere fitting does not guarantee that eq.4.8 can be considered as a universal theoretical line shape to explain the Raman spectra from a-Si. So in lieu of following the two fold approach we looked at the dependence of Raman

shift on the size of the nanowires. *Zi et al.* already proposed a set of parameters A and γ for the equation 4.4(a), which shows the size dependence of silicon column and spheres on the Raman shift. When we tried to find out the short range order for a widely studied peak of Raman spectra of a-Si at 480 cm^{-1} , assuming structure of the pseudo crystallite to be either columnar or spherical. The estimated size came out to be 2.9 and 6.1 \AA respectively. Considering the lattice parameter of silicon(5.43 \AA), if the short range order is more of a columnar shape than the size of it has to be 2.9 \AA , which means that not even a complete unit cell of silicon can be acquired by the structure and if it is more of spherical type than also only few unit cells can fit into that spherical shaped pseudo crystallite. This is more of a thermodynamically impossible situation to achieve. Because for a structure to be stable it should acquire at least required number of unit cells in it. So, this condition quickly clarifies the situation that one cannot use the same set of parameters as given in table 4.1 for a-Si as well.

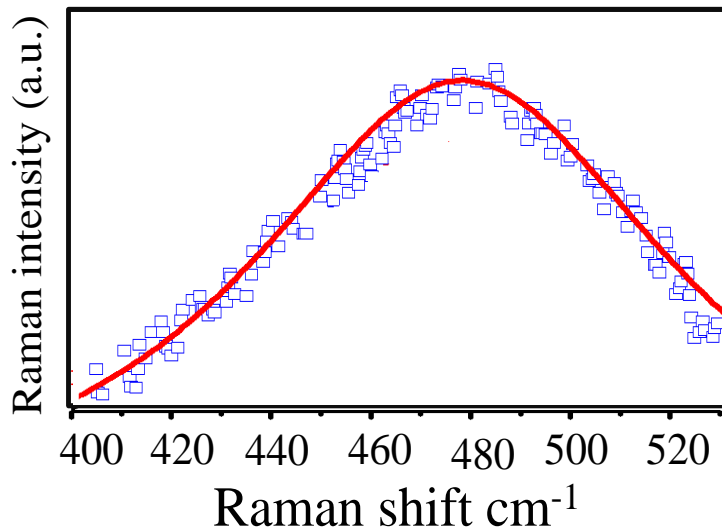


Figure4.10 Raman spectra of a-Si of samples AS2, discrete data points show the experimentally obtained Raman spectra whereas solid line corresponds to theoretical fitting (Eq. 4.8).

Keeping in mind the similarity in dependence of Raman shift on size in n-Si and a-Si. A similar set of parameters has been proposed for it, which is to be used exclusively for a-Si. The values are $A = 117 \text{ cm}^{-1}$ and $\gamma = 2.21$. Value of short range order estimated using the eq. 4.4(a) with the assigned valued of the parameters shows excellent agreement with the fitted Raman Spectra, hence validating the short range order.

The short range order for the above set of experimental data has been put in the form of table as shown below. The two data AS1 and AS2 are taken from the literature by Al-Salman R. *et al.*[43] and Lopez T. *et al.*[44]As from the above discussion it appears that the MPCM qualifies the requirement of the Raman scattering of a-Si to better extent via fitting and provides the fitting parameters such as size (short range order between a-Si). The Raman spectra AS1 and AS2 have been fitted using Eq. 4.4(a) by appropriately choosing the value of D (short range order). The solid line shown in Figure 4.9 shows the theoretically calculated Raman spectra using MPCM to fit the a-Si data of AS1 and AS2 respectively. The short range order present in a-Si and fitting parameters acquired by fitting the Raman scattering data using Eq. 4.4(a) is given in first four columns in Table 4.2.

Table 4.2:Raman parameters calculated from fitting of Raman spectra of AS1 and AS3 used in existing study. Values of D in the bracket in column four is the size estimated using Eq. 4.4(a).

Sample	Raman Peak position (cm^{-1})	FWHM (Γ) (cm^{-1})	Short range order D (\AA)
AS1(Al-Salman R. <i>et al.</i>)	477	108	8.3, (8.5)
AS2(Lopez T. <i>et al.</i>)	480	100	8.8, (8.8)

The size calculating from the fitting of experimental data from the two papers has been confirmed using equation 4.9 which comes out to be the same thereby validating the theory proposed.

The above mentioned discussion can be summarized by consolidating the line-shape representations for Si in its crystalline, nanocrystalline and amorphous phases as follows. Raman line-shape from c-Si is a typical Lorentian function and represented by one to result in a sharp symmetric line-shape centered at zone centered phonon frequency and show no size dependent peak shift. A shape and size dependent Raman line-shape asymmetry, red-shift and broadening is a typical behavior of Raman spectra obtained from nano-Si as represented by a spectral line-shape functioned worked out within the framework of PCM. Above mentioned two regimes of Si phases are well discussed in contrast to the a-Si phase in the context to Raman spectral line-shape representation. An asymmetric Raman line-shape obtained from a-Si can be successfully represented by MPCM and can be used to estimate short range order distance and phonon lifetime using Eq.4.8. In other words, Figure 4.10 depicts that phonon frequency for c-Si is constant (520 cm^{-1}), for nano Si it ranges from $520\text{-}510 \text{ cm}^{-1}$ and for a-Si shows transition from $480\text{-}470 \text{ cm}^{-1}$ respectively. Thus, a spectral line-shape (Eq. 4.8) and empirical relation (Eq. 4.4(a)) will empower one to quantify the distance up to which the order of crystallinity is intact in an a-Si[45,46]. As mentioned earlier, this can be of technological use because it is observed that the short range order in a-Si has an effect on the efficiency of a-Si solar cell and may have similar effect on other technological important properties of amorphous materials in general and a-Si in particular.

A Raman line-shape function proposed within the formulation of MPCM can be used to successfully represent experimental Raman spectrum obtained from a-Si. The line-shape thus obtained is validated by fitting

three different sets of a-Si Raman scattering data obtained by two different research groups from a-Si samples prepared by two different methods[35]. The Raman peak position is observed to be depending on a size parameter and has been used to quantify the distance of short range order present in a-Si. As an extension, an empirical relation between the short range order and Raman peak position has been proposed to be used as a handy tool for quantification of short range order. This relation, obtained based on BPM, seems to be universal in nature for quantification of short range order and can be used by a-Si prepared by any method. The line-shape fitting followed by proposed empirical relation allows one to have a complete set of Raman line-shape functions for the whole range of Si phases from crystalline to amorphous via nanocrystalline phase.

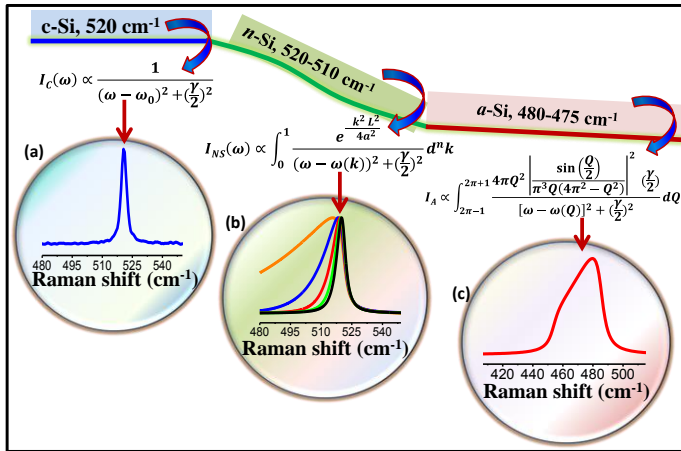


Figure 4.11 Theoretically obtained Raman line shapes for (a) c-Si, (b) SiNSs and (c) a-Si displayed in the different circles. The schematic (blue, green and red line on the top of Raman line shape) shows the abrupt transition from c-Si to a-Si

Chapter 5

New Findings and Results

5.1 Conclusions

The major conclusions of the research work reported in this thesis are summarized below:

- MPCM is not an appropriate theoretical model to explain the Raman line-shape from nanostructured materials in general and nanocrystalline silicon in particular.
- PCM is analyzed and it is found that it is well established and validated with regards to its appropriate physics involved in explaining the perturbation induced in the Raman spectrum of silicon.
- An alike theoretical model existing in case of c-Si and nano-Si has been proposed in case of a-Si, in order to understand the underlying physics in the Raman spectrum of a-Si.
- An attempt has been made for quantification of short-range order, a qualitative term till date, in amorphous materials .An equation has been proposed to estimate the short range of crystallinity in amorphous silicon.

5.3 Future Scope

- The theoretical model for amorphous silicon can be extended and developed in case of Ge, GaAs nanowires which can help in improving the efficiency of devices like solar cells.
- Study of size correlation between efficiency of amorphous silicon solar cell and its size distribution can be done, which will be useful in making the device more efficient to use.

- MPCM can be analyzed incorporating the effect of Fano resonance in the equation.

REFERENCES

- [1] Extremely Flexible Nanoscale Ultrathin Body Silicon Integrated Circuits on Plastic - Nano Letters (ACS Publications), (n.d.). <https://pubs.acs.org/doi/abs/10.1021/nl304310x> (accessed June 15, 2018).
- [2] M. Bruzzi, Novel Silicon Devices for Radiation Therapy Monitoring, Nucl. Instrum. Methods Phys. Res. Sect. Accel. Spectrometers Detect. Assoc. Equip. 809 (2016) 105–112. doi:10.1016/j.nima.2015.10.072.
- [3] A.G. Cullis, L.T. Canham, P.D.J. Calcott, The structural and luminescence properties of porous silicon, J. Appl. Phys. 82 (1997) 909–965. doi:10.1063/1.366536.
- [4] A.G. Cullis, L.T. Canham, Visible light emission due to quantum size effects in highly porous crystalline silicon, Nature. 353 (1991) 335–338. doi:10.1038/353335a0.
- [5] A. Nduwimana, X.-Q. Wang, Tunable electronic properties of silicon nanowires under strain and electric bias, AIP Adv. 4 (2014) 077122. doi:10.1063/1.4890674.
- [6] F. Maier-Flaig, J. Rinck, M. Stephan, T. Bocksrocker, M. Bruns, C. Kübel, A.K. Powell, G.A. Ozin, U. Lemmer, Multicolor Silicon Light-Emitting Diodes (SiLEDs), Nano Lett. 13 (2013) 475–480. doi:10.1021/nl3038689.
- [7] V. Kveder, M. Badylevich, E. Steinman, A. Izotov, M. Seibt, W. Schröter, Room-temperature silicon light-emitting diodes based on dislocation luminescence, Appl. Phys. Lett. 84 (2004) 2106–2108. doi:10.1063/1.1689402.
- [8] J. von Behren, T. van Buuren, M. Zacharias, E.H. Chimowitz, P.M. Fauchet, Quantum confinement in nanoscale silicon: The correlation of size with bandgap and luminescence, Solid State Commun. 105 (1998) 317–322. doi:10.1016/S0038-1098(97)10099-0.
- [9] Tailoring Optical Properties of Silicon Nanowires by Au Nanostructure Decorations: Enhanced Raman Scattering and Photodetection - The Journal of Physical Chemistry C (ACS Publications), (n.d.). <https://pubs.acs.org/doi/abs/10.1021/jp210198u> (accessed June 15, 2018).
- [10] H. Yoshioka, N. Morioka, J. Suda, T. Kimoto, Bandgap shift by quantum confinement effect in $\langle 100 \rangle$ Si-nanowires derived from threshold-voltage shift of fabricated metal-oxide-semiconductor field effect transistors and theoretical calculations, J. Appl. Phys. 109 (2011) 064312. doi:10.1063/1.3559265.
- [11] Semiconductor Nanowire Fabrication by Bottom-Up and Top-Down Paradigms - Chemistry of Materials (ACS Publications), (n.d.).

- <https://pubs.acs.org/doi/abs/10.1021/cm300570n> (accessed June 15, 2018).
- [12] Simple aspects of Raman scattering - The Journal of Physical Chemistry (ACS Publications), (n.d.).
<https://pubs.acs.org/doi/abs/10.1021/j100207a018> (accessed June 15, 2018).
- [13] Fano Scattering: Manifestation of Acoustic Phonons at the Nanoscale - The Journal of Physical Chemistry Letters (ACS Publications), (n.d.).
<https://pubs.acs.org/doi/abs/10.1021/acs.jpcllett.6b02090> (accessed June 15, 2018).
- [14] P. Yogi, D. Poonia, S. Mishra, S.K. Saxena, S. Roy, V. Kumar, P.R. Sagdeo, R. Kumar, Spectral Anomaly in Raman Scattering from p-Type Silicon Nanowires, *J. Phys. Chem. C*. 121 (2017) 5372–5378. doi:10.1021/acs.jpcc.6b12811.
- [15] C.-Y. Meng, J.-L. Chen, S.-C. Lee, C.-T. Chia, Doping effects on the Raman spectra of silicon nanowires, *Phys. Rev. B*. 73 (2006) 245309. doi:10.1103/PhysRevB.73.245309.
- [16] E. Anastassakis, A. Pinczuk, E. Burstein, F.H. Pollak, M. Cardona, Effect of static uniaxial stress on the Raman spectrum of silicon, *Solid State Commun.* 8 (1970) 133–138. doi:10.1016/0038-1098(70)90588-0.
- [17] R. Kumar, G. Sahu, S.K. Saxena, H.M. Rai, P.R. Sagdeo, Qualitative Evolution of Asymmetric Raman Line-Shape for NanoStructures, *Silicon*. 6 (2014) 117–121. doi:10.1007/s12633-013-9176-9.
- [18] C. Smit, R. a. C.M.M. van Swaaij, H. Donker, A.M.H.N. Petit, W.M.M. Kessels, M.C.M. van de Sanden, Determining the material structure of microcrystalline silicon from Raman spectra, *J. Appl. Phys.* 94 (2003) 3582–3588. doi:10.1063/1.1596364.
- [19] J. Zi, K. Zhang, X. Xie, Comparison of models for Raman spectra of Si nanocrystals, *Phys. Rev. B*. 55 (1997) 9263–9266. doi:10.1103/PhysRevB.55.9263.
- [20] J. Zi, H. Büscher, C. Falter, W. Ludwig, K. Zhang, J. Zi, Raman shifts in Si nanocrystals, *Appl. Phys. Lett.* 69 (1996) 200–202. doi:10.1063/1.117371.
- [21] P.W. Chapman, O.N. Tufte, J.D. Zook, D. Long, Electrical Properties of Heavily Doped Silicon, *J. Appl. Phys.* 34 (1963) 3291–3295. doi:10.1063/1.1729180.
- [22] N. Tit, M.W.C. Dharma-wardana, Quantum confinement and direct-bandgap character of Si/SiO₂ superlattices, *Solid State Commun.* 106 (1998) 121–126. doi:10.1016/S0038-1098(98)00047-7.
- [23] L. Sun, Y. Fan, X. Wang, R.A. Susantyoko, Q. Zhang, Large scale low cost fabrication of diameter controllable silicon nanowire arrays,

- Nanotechnology. 25 (2014) 255302. doi:10.1088/0957-4484/25/25/255302.
- [24] S.K. Saxena, G. Sahu, P. Yogi, P.R. Sagdeo, R. Kumar, Spectroscopic Investigation of well aligned Silicon Nano wires Fabricated by Metal Induced Etching, *Mater. Today Proc.* 3 (2016) 1835–1839. doi:10.1016/j.matpr.2016.04.082.
- [25] W.-K. To, C.-H. Tsang, H.-H. Li, Z. Huang, Fabrication of n-Type Mesoporous Silicon Nanowires by One-Step Etching, *Nano Lett.* 11 (2011) 5252–5258. doi:10.1021/nl202674t.
- [26] Role of metal nanoparticles on porosification of silicon by metal induced etching (MIE) - ScienceDirect, (n.d.). <https://www.sciencedirect.com/science/article/pii/S074960361630146X?via%3Dihub> (accessed June 15, 2018).
- [27] H. Richter, Z.P. Wang, L. Ley, The one phonon Raman spectrum in microcrystalline silicon, *Solid State Commun.* 39 (1981) 625–629. doi:10.1016/0038-1098(81)90337-9.
- [28] G. Gouadec, P. Colomban, Raman Spectroscopy of nanomaterials: How spectra relate to disorder, particle size and mechanical properties, *Prog. Cryst. Growth Charact. Mater.* 53 (2007) 1–56. doi:10.1016/j.pcrysgrow.2007.01.001.
- [29] S. Piscanec, M. Cantoro, A.C. Ferrari, J.A. Zapien, Y. Lifshitz, S.T. Lee, S. Hofmann, J. Robertson, Raman spectroscopy of silicon nanowires, *Phys. Rev. B.* 68 (2003) 241312. doi:10.1103/PhysRevB.68.241312.
- [30] V. Paillard, P. Puech, M.A. Laguna, R. Carles, B. Kohn, F. Huisken, Improved one-phonon confinement model for an accurate size determination of silicon nanocrystals, *J. Appl. Phys.* 86 (1999) 1921–1924. doi:10.1063/1.370988.
- [31] İ. Doğan, M.C.M. van de Sanden, Direct characterization of nanocrystal size distribution using Raman spectroscopy, *J. Appl. Phys.* 114 (2013) 134310. doi:10.1063/1.4824178.
- [32] X. Jia, Z. Lin, T. Zhang, B. Puthen-Veetil, T. Yang, K. Nomoto, J. Ding, G. Conibeer, I. Perez-Wurfl, Accurate analysis of the size distribution and crystallinity of boron doped Si nanocrystals via Raman and PL spectra, *RSC Adv.* 7 (2017) 34244–34250. doi:10.1039/C7RA04472K.
- [33] I.H. Campbell, P.M. Fauchet, The effects of microcrystal size and shape on the one phonon Raman spectra of crystalline semiconductors, *Solid State Commun.* 58 (1986) 739–741. doi:10.1016/0038-1098(86)90513-2.
- [34] R. Epur, P.J. Hanumantha, M.K. Datta, D. Hong, B. Gattu, P.N. Kumta, A simple and scalable approach to hollow silicon nanotube (h-SiNT) anode architectures of superior electrochemical stability and reversible capacity, *J. Mater. Chem. A.* 3 (2015) 11117–11129. doi:10.1039/C5TA00961H.

- [35] M. Tanwar, P. Yogi, S. Lambora, S. Mishra, S.K. Saxena, P.R. Sagdeo, A.S. Krylov, R. Kumar, Generalisation of phonon confinement model for interpretation of Raman line-shape from nano-silicon, *Adv. Mater. Process. Technol.* 4 (2018) 227–233. doi:10.1080/2374068X.2017.1413527.
- [36] Raman spectroscopy of amorphous and microcrystalline silicon films deposited by low-pressure chemical vapor deposition: *Journal of Applied Physics*: Vol 78, No 12, (n.d.). <https://aip.scitation.org/doi/10.1063/1.360468> (accessed June 15, 2018).
- [37] D. Gracin, K. Juraić, J. Sancho-Parramon, P. Dubček, S. Bernstorff, M. Čeh, Amorphous-Nano-Crystalline Silicon Thin Films in Next Generation of Solar Cells, *Phys. Procedia.* 32 (2012) 470–476. doi:10.1016/j.phpro.2012.03.587.
- [38] D.E. Carlson, C.R. Wronski, Amorphous silicon solar cell, *Appl. Phys. Lett.* 28 (1976) 671–673. doi:10.1063/1.88617.
- [39] Optically enhanced amorphous silicon solar cells: *Applied Physics Letters*: Vol 42, No 11, (n.d.). <https://aip.scitation.org/doi/10.1063/1.93817> (accessed June 15, 2018).
- [40] H.K. Charles, A.P. Ariotedjo, Review of amorphous and polycrystalline thin film silicon solar cell performance parameters, *Sol. Energy.* 24 (1980) 329–339. doi:10.1016/0038-092X(80)90294-7.
- [41] L.S. Froufe-Pérez, M. Engel, P.F. Damasceno, N. Muller, J. Haberko, S.C. Glotzer, F. Scheffold, Role of Short-Range Order and Hyperuniformity in the Formation of Band Gaps in Disordered Photonic Materials, *Phys. Rev. Lett.* 117 (2016) 053902. doi:10.1103/PhysRevLett.117.053902.
- [42] R. Tsu, R.T. Hodgson, T.Y. Tan, J.E. Baglin, Order-Disorder Transition in Single-Crystal Silicon Induced by Pulsed uv Laser Irradiation, *Phys. Rev. Lett.* 42 (1979) 1356–1358. doi:10.1103/PhysRevLett.42.1356.
- [43] R. Al-Salman, J. Mallet, M. Molinari, P. Fricoteaux, F. Martineau, M. Troyon, S.Z.E. Abedin, F. Endres, Template assisted electrodeposition of germanium and silicon nanowires in an ionic liquid, *Phys. Chem. Chem. Phys.* 10 (2008) 6233–6237. doi:10.1039/B809075K.
- [44] T. Lopez, L. Mangolini, Low activation energy for the crystallization of amorphous silicon nanoparticles, *Nanoscale.* 6 (2014) 1286–1294. doi:10.1039/C3NR02526H.
- [45] From Crystals to Disordered Crystals: A Hidden Order-Disorder Transition | *Scientific Reports*, (n.d.). <https://www.nature.com/articles/srep15378> (accessed June 15, 2018).
- [46] W.-E. Hong, J.-S. Ro, Kinetics of solid phase crystallization of amorphous silicon analyzed by Raman spectroscopy, *J. Appl. Phys.* 114 (2013) 073511. doi:10.1063/1.4818949.

- [47] P. Yogi, M. Tanwar, S.K. Saxena, S. Mishra, D.K. Pathak, A. Chaudhary, P.R. Sagdeo, R. Kumar, Quantifying the Short-Range Order in Amorphous Silicon by Raman Scattering, *Anal. Chem.* (2018). doi:10.1021/acs.analchem.8b01352.
- [48] F. Cerdeira, T.A. Fjeldly, M. Cardona, Effect of Free Carriers on Zone-Center Vibrational Modes in Heavily Doped β -type Si. II. Optical Modes, *Phys. Rev. B.* 8 (1973) 4734–4745. doi:10.1103/PhysRevB.8.4734.
- [49] Confined Phonons in Si Nanowires - Nano Letters (ACS Publications), (n.d.). <https://pubs.acs.org/doi/abs/10.1021/nl0486259> (accessed June 15, 2018).
- [50] S.K. Saxena, P. Yogi, S. Mishra, H.M. Rai, V. Mishra, M.K. Warshi, S. Roy, P. Mondal, P.R. Sagdeo, R. Kumar, Amplification or cancellation of Fano resonance and quantum confinement induced asymmetries in Raman line-shapes, *Phys. Chem. Chem. Phys.* 19 (2017) 31788–31795. doi:10.1039/C7CP04836J.
- [51] S. Vepřek, Z. Iqbal, F.-A. Sarott, A thermodynamic criterion of the crystalline-to-amorphous transition in silicon, *Philos. Mag. B.* 45 (1982) 137–145. doi:10.1080/13642818208246392.
- [52] A novel low temperature vapor phase hydrolysis method for the production of nano-structured silica materials using silicon tetrachloride - RSC Advances (RSC Publishing), (n.d.). <http://pubs.rsc.org/en/Content/ArticleLanding/2014/RA/c3ra47018k#!divAbstract> (accessed June 15, 2018).
- [53] K.W. Adu, H.R. Gutiérrez, U.J. Kim, P.C. Eklund, Inhomogeneous laser heating and phonon confinement in silicon nanowires: A micro-Raman scattering study, *Phys. Rev. B.* 73 (2006) 155333. doi:10.1103/PhysRevB.73.155333.
- [54] K. Jarolimek, E. Hazrati, R.A. de Groot, G.A. de Wijs, Band Offsets at the Interface between Crystalline and Amorphous Silicon from First Principles, *Phys. Rev. Appl.* 8 (2017) 014026. doi:10.1103/PhysRevApplied.8.014026.
- [55] Y. Zhao, X. Liu, H. Li, T. Zhai, H. Zhou, Hierarchical micro/nano porous silicon Li-ion battery anodes, *Chem. Commun.* 48 (2012) 5079–5081. doi:10.1039/C2CC31476B.
- [56] Field-Effect Transistors Based on Silicon Nanowire Arrays: Effect of the Good and the Bad Silicon Nanowires - ACS Applied Materials & Interfaces (ACS Publications), (n.d.). <https://pubs.acs.org/doi/abs/10.1021/am300961d> (accessed June 15, 2018).